Vibrational Spectroscopy 74 (2014) 20–32

Contents lists available at ScienceDirect

Vibrational Spectroscopy

journal homepage: www.elsevier.com/locate/vibspec

Molecular mechanics investigation of some acrylic polymers using SPASIBA force field

M.O. Bensaid[a,*], L. Ghalouci[a], S. Hiadsi[a], F. Lakhdari[b], N. Benharrats[b], G. Vergoten[c]

[a] Laboratoire de Microscope Electronique et Science des Matériaux, Université des Sciences et de la Technologie d'Oran Mohamed Boudiaf, B.p 1505 El M'Naouar, 31000 Oran, Algeria
[b] Laboratoire des Matériaux Mixtes, Université des Sciences et de la Technologie d'Oran Mohamed Boudiaf, Algeria
[c] UMR CNRS8576 "Glycobiologie Structurale et Fonctionnelle", Université des Sciences et Technologies de Lille, 59655 Villeneuve d'Ascq Cedex, France

ARTICLE INFO

Article history:
Received 17 April 2014
Received in revised form 2 July 2014
Accepted 3 July 2014
Available online 11 July 2014

Keywords:
Force field
SPASIBA
Acrylic polymers
Potential energy distribution
Vibrational analysis

ABSTRACT

The First generation SPASIBA force field is used to study normal vibrational modes of PMMA, and then extended to other thermoplastic polymers, namely PMA, PMAA and PAA, in order to determine its parameters transferability. To this end, FTIR and FTR spectra of pure PMMA samples, prepared by the emulsion polymerization of MMA and initiated by sodium, are recorded in 400–3500 cm^{-1} and 200–3500 cm^{-1}, respectively. A detailed vibrational analysis was performed on the obtained spectra and the observed frequencies are assigned to their respective vibrational modes, supported by potential energy distribution (PED) analysis. Our numerical results reveal an RMS value of 7.8 cm^{-1} corresponding to IR wavenumbers and 8.7 cm^{-1} relatively to Raman wavenumbers. Our vibrational calculations on PMA, PMAA and PAA polymers reveal that the parameters transferability criterion, established by Shimanouchi, is verified for the SPASIBA force field.

1. Introduction

The molecular modeling of acrylic polymers has recently attracted much interest due to their outstanding properties such as high electrical resistivity, low water absorption, fair tensile strength and excellent optical characteristics as well as commercial importance [1]. The Poly Methyl methacrylate (PMMA) polymer offers a particular regard since it easily allows studying different physical properties related to polymers [2]. PMMA is also the most used member, among a set of thermoplastic polymers, in wide variety of applications in virtue of its excellent transparency and good mechanical and chemical properties [3–6]. X-ray diffraction techniques are the most commonly applied complementary discipline to microscopy for structural studies. For example, the atomic position (at least for the heavier atoms) and geometrical parameters can be obtained from X-ray diffraction experiment. However, when addressing vibrational modes study, X-ray diffraction is not able to probe vibrational sensitive modes of chemical structures. Both polymer configuration and conformational sensitive modes can be probed by means of vibrational spectroscopy tool [7,8]. This later helps a lot to understand the dynamical behavior of a polymer chain. Therefore, Infrared and Raman spectroscopies remain the most important and common techniques available in research and industrial laboratories. Compared to experimental vibrational data, ab-initio/dft methods give very good reproduction of wavenumbers assignments of the fundamentals bands for small molecules. However, for large molecules (i.e., with more than 100 atoms) one needs a very powerful computer. With larger molecules, the time required for computation becomes prohibitively large, and one must resort to more approximate methods such as molecular mechanics force field approach. Nowadays, there is a variety of force fields dedicated to thermoplastic polymers. The best known for atomistic simulation of polymeric systems, are COMPASS [9], CVFF [10], PCFF [11] and DREIDING [12] for polyethylene oxide, TRIPOS 5.2 [13] for polyrotaxanes, CHARMM [14] and AMBER [15] for polystyrene and GROMOS [16] for polypyrrole. For biomolecular systems, CHARMM, AMBER and SPASIBA (Spectroscopic Potential Algorithm for Simulating Biomolecular Conformational Adaptability) seem to be the most appropriate force fields. SPASIBA consists of a pairing between a molecular mechanics force field derived from the AMBER package [17] and the Urey–Bradley–Shimanouchi (UBS) spectroscopic force field [18].

Compared to the others force fields of second generation (e.g. PCFF, COMPASS, ...) which combine bonded terms, non-bonded terms and cross terms to make more accurate theirs vibrational analysis results, SPASIBA like first generation force field replaces

* Corresponding author. Tel.: +213 776 43 94 02.
E-mail address: bwassini@yahoo.fr (M.O. Bensaid).

http://dx.doi.org/10.1016/j.vibspec.2014.07.001
0924-2031/

the cross terms (difficult to parameterized) by UBS constants terms for bond lengths and bond angles. This makes it an accurate force field and simple to handle for vibrational analysis studies. Literature survey reveals that SPASIBA was already parameterized for lipids [19], proteins, oligosaccharides and glycoprotein [20], aliphatic amino acids [21], alkanes [22], alkenes [23], chondroitin sulfate [24], aliphatic ethers [25], alcohols [26] and esters [27]. However, to the best of our knowledge, the accuracy of this force field has not been tested yet on thermoplastic polymers (except for polyaniline (PANI) [28]) in contrast to CHARMM and AMBER. Hence, the aim of this work is to fill this breach in literature by conducting a SPASIBA force field study on some thermoplastic polymers, namely PMMA, PMA, PMAA and PAA. This paper is organized as follows: in Section 2, experimental procedure to determine Infrared and Raman vibrational frequencies of PMMA is described. Section 3 exposes the adopted computational method. In Section 4, we present and discuss our experimental and numerical results on the light of previous works followed by a conclusion.

2. Experimental procedure

Purified and distilled methyl methacrylate (Aldrich, USA) was used for the polymer's preparation. The powder of the PMMA was synthetized with a radical reaction process based on the emulsion polymerization of the methyl methacrylate using sodium persulphate as initiator and sodium dodecyl sulfate as emulsifying agent at 80 °C. Each PMMA pellet was prepared by mixing 1 mg of the powdered sample with 100 mg of dried potassium bromide powder. The mixture was carried out using a pestle and agate mortar, and then pressed in a special die up to a pressure of 700 kg/cm^2 to yield a transparent disk. The Fourier Transform Infrared (FTIR) spectrum of the PMMA polymer was recorded in the range 400–3500 cm^{-1} using a Nicolet Avatar 360 Fourier Transform Infrared Spectrometer. The scanning speed was held at 30 cm^{-1} min^{-1} with a spectral width of 20 cm^{-1}. Frequencies of all sharp bands are within a resolution of ± 2 cm^{-1}. The Fourier Transform Raman (FTR) spectrum of our PMMA sample (pumped by 532 nm laser light) was recorded in the range 200–3500 cm^{-1} with a resolution of 2 cm^{-1} using a LabRam Xplora confocal Raman microscope (Horiba Jobin Yvon) equipped with a confocal microscope (Olympus BX51). The FTIR and FTR spectra obtained are used as an experimental basis to establish the PMMA molecule force field through normal coordinate analysis.

3. Computational method

We first conducted a vibrational analysis on a PMMA polymer chain with 100 monomers of 15 atoms each. The followed computational method is well described in Refs. [20,29]. In our calculations, the dielectric constant is used equal to 1. The 1–4 Van der Waals interactions and the full 1–4 electrostatic potential have been chosen to describe the non-bonded interactions in our polymer. The SPASIBA force field constants for organic molecules [22,23,25–27] are used as starting point to determine our new PMMA structure parameters. These constants are refined to obtain the best fit between the calculated frequencies and their corresponding peaks observed in the FTIR/FTR spectra, and then transferred to acrylic acid derivatives in order to analyze their vibrational normal modes and their assignments using PED analysis. To investigate the force field parameters accuracy of the considered polymer, the root mean square (RMS) values between calculated and observed wavenumbers are estimated using the following expression:

$$\mathrm{RMS} = \sqrt{\frac{1}{n}\sum_{i}^{n}\left(\nu_i^{\mathrm{calc}} - \nu_i^{\mathrm{exp}}\right)^2} \quad (1)$$

We can summarize the force constants optimization and normal modes analysis procedure according to the following steps:

1. The monomer of each polymer chain used in our simulation was generated initially by the GAUSSIAN 98 program [30]. The starting monomer structure was optimized using quantum mechanics at the Hartree–Fock level with 6–31G** basis set in order to calculate the partial charges. Each monomer was then exported to the SPASIBA force field program where they were propagated 100 times to obtain our initial structures (PMMA, PMAA, PMA and PAA) destined to be optimized by the SPASIBA force field program.
2. Determination of the force field parameters which reproduce the available experimental vibrational spectra. The optimized SPASIBA parameters employed in the present work are shown in Table 1(a)–(d).
3. Computation of the polymer geometry with the lower energy using switched steepest descent to conjugate gradient method. The convergence is reached when the total force becomes less than 10^{-5} kcal mol^{-1} Å^{-1}.
4. Determination of the fundamental vibrations supported by normal coordinates analysis and PED calculations.
5. Transferability evaluation of the SPASIBA force field constants to the other acrylic polymers, namely PMA, PMAA and PAA.

The repeating units of acrylic polymers with their SPASIBA atom types are presented in Fig. 1(a)–(d). The four structures have the same backbone configuration and different side chain.

Derreumaux and Vergoten [20] reported that the equilibrium bond lengths are explicitly expressed in the UBS bond angle energy to improve the transferability of the bending force constant from one molecule to another. The SPASIBA Force field parameters are determined from normal modes analysis. A set of 39 independent force constants were considered as starting parameters (see Table 1(a)–(d)) and were refined by adjustment procedures to obtain the best average difference between the calculated and observed values. We notice that the specific Urey–Bradley–Shimanouchi force constants Kappa, LCH_2 and trans-gauche used in this work and originated directly from Ref. [20] are not given here. The final empirical set of SPASIBA parameters deduced from the vibrational analysis is displayed in Table 1(a)–(d) and might be considered as database for further polymeric studies.

4. Results and discussion

4.1. Assignments for the infrared and Raman spectra

Our observed FTIR and FTR spectra are given in Figs. 2 and 3, respectively. The FTIR spectrum in Fig. 2 is characterized by two intense peaks relative to stretching carbonyl group vibration (C=O) at 1730 cm^{-1} and stretching ester group vibration (C—O) at 1149 cm^{-1}. In the [3000–2854] cm^{-1} range the (C—H) groups exhibit stretching modes, whereas in the [1485–1387] cm^{-1} range the (C—H) groups exhibit deformation mode. The weak peak at 1060 cm^{-1} is due to the (OCH_3) rocking mode. The broad peak ranging from 1260 to 1000 cm^{-1} is attributed to the stretching vibration of the (C—O) ester bond. The peaks at 989 and 966 cm^{-1} correspond respectively to (O—CH_3) symmetric stretching and CH_3 rocking. The FTR spectrum in Fig. 3 shows several narrow peaks, specific to

Table 1
Empirical SPASIBA force constants related to acrylic polymers.

(a) Parameters of bonding energetic term for SPASIBA force field

Bonds	Starting parameters		Refined parameters	
	K (kcal mol^{-1})	R_0 (Å)	K (kcal mol^{-1})	R_0 (Å)
CT—HC	320.0[b]	1.110[b]	325.0	1.110
C—OE	310.0[f]	1.360[f]	335.0	1.364
C=O	615.0[b]	1.236[b]	760.0	1.236
CT—OE	245.0[f]	1.470[f]	345.0	1.430
CT—C	160.7[b]	1.506[b]	190.0	1.506
CT—CT	165.0[b]	1.530[b]	165.0	1.530
CT—C9	165.0[c]	1.530[c]	165.0	1.530
C9—HM	291.3[c]	1.110[c]	308.5	1.110
HE—OE[g]	536.0[b]	0.950[b]	565.5	0.960

(b) Parameters for valence energetic term for SPASIBA force field

Valence angle	Starting parameters			Refined parameters		
	H (kcal mol^{-1} rad^{-2})	θ_0 (°)	F (kcal mol^{-1} Å^2)	H (kcal mol^{-1} rad^{-2})	θ_0 (°)	F (kcal mol^{-1} Å^2)
HM—C9—HM	29.60[c]	107.70[c]	10.50[c]	30.00	108.50	10.07
OE—CT—HC	17.50[e]	109.00[e]	120.00[e]	20.55	109.50	57.70
HC—CT—HC	29.60[d]	108.50[d]	10.07[d]	29.00	108.70	10.07
C—OE—CT	30.00[f]	114.00[f]	30.00[f]	20.30	117.00	100.50
O=C—CT	14.00[c]	123.60[c]	35.00[c]	21.58	126.50	58.14
C—CT—C9	18.70[b]	111.80[b]	47.47[b]	18.70	111.80	47.47
O=C—OE	65.00[f]	125.00[f]	100.00[f]	59.70	126.00	120.50
CT—C—OE	40.00[f]	112.20[f]	100.00[f]	20.30	113.00	80.50
CT—CT—CT	18.70[b]	111.80[b]	47.47[b]	18.70	111.80	47.47
CT—CT—C9	18.70[b]	111.80[b]	47.47[b]	18.70	111.80	47.47
CT—C9—CT	18.70[b]	111.80[b]	47.47[b]	18.70	111.80	47.47
CT—C9—HM	15.10[c]	109.50[c]	69.40[c]	14.10	109.40	70.00
CT—CT—HC	15.89[b]	109.50[b]	69.43[b]	15.89	109.50	69.43
C9—CT—HC	15.90[a]	109.50[a]	69.40[a]	14.90	109.40	69.90
CT—CT—C	20.14[b]	106.50[b]	47.47[b]	20.14	106.50	47.47
HC—CT—C	15.65[b]	109.50[b]	78.37[b]	15.65	109.50	78.37
C9—CT—C9	18.70[c]	111.80[c]	47.50[c]	18.70	111.80	47.47
C—CT—HC[h]	16.00[b]	109.50[b]	77.00[b]	15.65	109.50	78.37
C—OE—HE[i]	28.45[b]	107.00[b]	41.00[b]	28.50	110.00	41.00

(c) Dihedral angle energetic term for SPASIBA force field

Torsions	Starting parameters			Refined parameters		
	$Vn/2$ (kcal mol^{-1})	Phase (°)	n (order)	$Vn/2$ (kcal mol^{-1})	Phase (°)	n (order)
X—CT—C9—X	0.160[b]	1[b]	0[b]	0.160	0	1
X—CT—C=O	0.130[f]	0[f]	3[f]	0.550	0	3
X—C—OE—X	3.330[f]	180[f]	2[f]	1.500	180	2
X—CT—OE—X	0.010[f]	0[f]	3[f]	0.300	0	3
X—CT—CT—X	0.150[d]	0[d]	3[d]	1.300	0	3
X—C—CT—X	0.250[d]	180[d]	2[d]	0.550	0	3
CT—OE—C—CT	-1.175[f]	180[f]	2[f]	1.500	180	2
X—OE—C—X	3.330[f]	180[f]	2[f]	1.500	180	2
CT—CT—C=O	0.130[f]	0[f]	3[f]	0.067	180	3
C—OE—CT—HC	0.270[f]	0[f]	3[f]	0.900	0	3

(d) Out of plane bending term for SPASIBA force field

Torsions	Started parameters			Refined parameters		
	$Vn/2$ (kcal mol^{-1})	Phase (°)	n (order)	$Vn/2$ (kcal mol^{-1})	Phase (°)	n (order)
X—X—C=O	12[f]	180[f]	2[f]	11	180	3

[a] Ref. [19].
[b] Ref. [20].
[c] Ref. [21].
[d] Ref. [24].
[e] Ref. [25].
[f] Ref. [27].
[g] For PAA and PMAA.
[h] For PMAA.
[i] For PAA.

the PMMA chain. In the [3000–2800] cm^{-1} range the Raman transitions are the most prominent and are identified as (C—H) stretching vibrations of CH_2 and CH_3. The peak at 1729 cm^{-1} corresponds to (C=O) stretching vibration. The [1481–1453] cm^{-1} range is dominated by (C—H) bending vibration, whereas [1288–813] cm^{-1} range corresponds to (C—O) stretching vibration. The (CH_2) wagging and twisting vibrations at 1406 and 1324 cm^{-1}, the (C—Cα) stretching vibrations at 1124 cm^{-1}, the (CH_3)

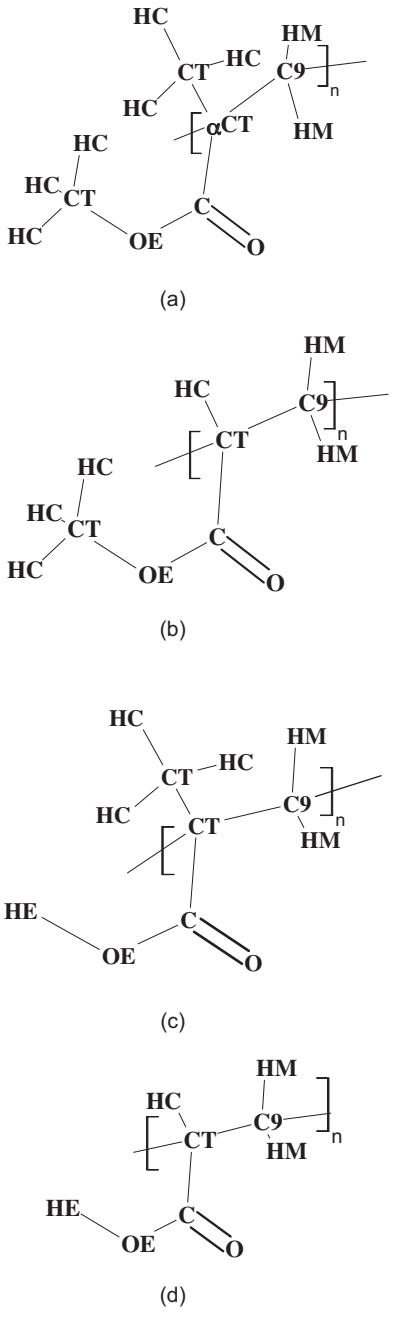

Fig. 1. Monomer units and SPASIBA atom types of (a) poly(methyl methacrylate) [PMMA], (b) poly(methyl acrylate) [PMA], (c) poly(methacrylic acid) [PMAA], and (d) poly(acrylic acid) [PAA].

twisting mode at 1044 cm^{-1}, the (C–C=O) in-plane bending vibrations at 600 and 559 cm^{-1} and the (O–C=O) deformation vibrations at 454 cm^{-1} are only observed in FTR spectrum. Our FTIR and FTR spectra confirm the presence of all functional groups specific to the PMMA polymer. We note that most bands identified in our FTIR and FTR spectra are already reported in references [31–36].

4.2. Optimized geometrical parameters

Small models can be minimized to a global minimum. However, multiple minimizations from different starting conformations should be run to confirm that a global minimum has indeed been found. Larger models like our systems can often be minimized to several different conformations that a molecule might assume at

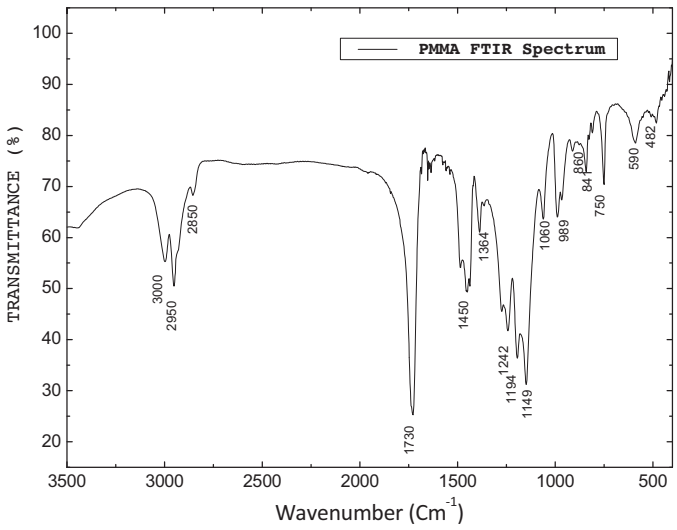

Fig. 2. The observed FTIR spectrum of PMMA.

0 K. But, a global minimum may never be found for these large models, because of the complexity of the potential energy surface. In our case, unfortunately, there is no guarantee that the minimum we have found is necessarily a global minimum, but by comparing our results with other experimental and theoretical ones (especially those of Vacatello and Flory [43]) we can say that we have reached a good minimum.

The optimized geometrical parameters (bond lengths, valence and dihedral angles) of our studied PMMA polymer are summarized in Table 2, using SPASIBA atom types notations given in Fig. 1. Our PMMA bond lengths, valence angles and dihedral angles respectively present average deviations of 0.006 Å, 0.3° and 1.4° compared to literature values given in Table 2.

The conformational isomers generated by rotation around the X–C9–CT–X bond determines the conformational structure of the chain backbone (trans(t) and gauche(g)), whereas, the rotation around the X–CT–C–X bond determines the orientation of the ester groups relatively to the chain.

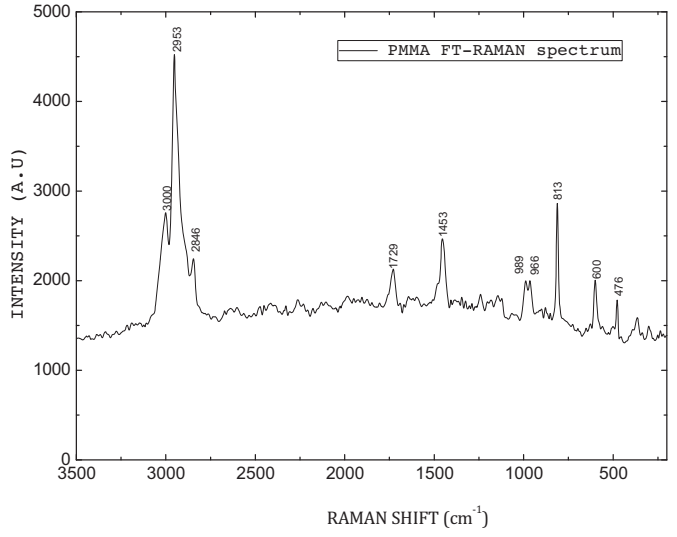

Fig. 3. The observed FTR spectrum of PMMA recorded from the central area.

Table 2
Mean value geometrical parameters of PMMA optimized by SPASIBA force field along with other experimental and theoretical results. Bonds are given in Å and valence and dihedral angles in degrees.

Parameters	Our results	Other works
CT—HC	1.110	1.10[a,g], 1.08[c]
C—OE	1.354	1.31[c], 1.36[b,e,f,g], 1.37[d]
C=O	1.203	1.19[c], 1.21[a], 1.22[b,e,f,g], 1.27[d]
CT—OE	1.429	1.39[d], 1.46[a], 1.45[b,e,f,g], 1.42[c]
CT—C	1.540	1.32[a], 1.49[d], 1.52[e,f,g]
CT—CT	1.530	1.52[c], 1.53[b,d,e,f,g]
CT—C9	1.530	1.53[b,d,e,f,g]
C9—HM	1.115	1.08[c], 1.10[g]
HM—C9—HM	106.25	107.5[g], 120[c]
OE—CT—HC	110.21	–
HC—CT—HC	108.93	108[c], 109[c], 107.5[g]
C—OE—CT	118.32	110[f], 112.4[a], 114.0[b], 116[c], 117[d]
O=C—CT	123.35	121.0[b,e], 122[f,g], 124.0[c], 125[d]
C—CT—C9	108.79	109.5[b,d,e], 111[f]
O=C—OE	123.88	124.0[a,f,g], 122[c]
CT—C—OE	112.36	114.0[b,e,f,g], 113[c]
CT—CT—CT	110.79	110[b,c], 109[c], 111[g]
CT—CT—C9	114.75	122.0[b], 115.25[d]
CT—C9—CT	124.03	113.0[e], 124.0[a,f], 122.0[b,d]
CT—C9—HM	105.74	–
CT—CT—HC	111.24	109.5[g]
CT—CT—C	109.89	109[c], 110[c]
C9—CT—C9	111.69	106[f], 109[c], 109.5[d], 114.0[a], 110.0[b,c,d,e]
X—CT—C9—X	−25.12, 13.12	−23, 11[g], −22, 12[g]
X—CT—C—X	−11.15, 174.13	−8[g], 171[g]

[a] Ref. [37].
[b] Ref. [38].
[c] Ref. [39].
[d] Ref. [40].
[e] Ref. [41].
[f] Ref. [42].
[g] Ref. [43].

Our PMMA dihedral angles values corroborate well with the results of Vaccatelo and Flory [43]. Thus, we can conclude that our polymer is of *tt* sequence with (10/1) helix conformation.

From Table 2, we can state that our optimized geometrical parameters of PMMA polymer are in good agreement with literature results, and can be taken into account for the vibrational analysis and assignments.

4.3. Normal mode analysis

We have carried out the normal mode vibrations analysis using the SPASIBA force field refined constants. Table 3 summarizes the PMMA infrared and Raman frequencies, their relative intensities and the calculated vibrational frequencies using PED analysis. We note that redundant modes and PED contributions below 10% are omitted. The R.M.S deviations between the predicted and observed wavenumbers from infrared and Raman frequencies are 7.8 and 8.7 cm^{-1}, respectively.

In the 3000–2800 cm^{-1} range

The vibrations in this region refer to the (C—H) stretching modes in PMMA structure. The (C—H) stretching vibrations of PMMA are attributable to three distinct constituent groups: the α-methyl group directly attached to main chain carbon, the side chain ester methyl group and the backbone methylene group. The literature assignments of these broadened and highly overlapped bands lead to lack of distinctness between αCH_3, OCH_3 and CH_2 groups. The seven bands, generally reported in infrared and Raman spectra [46,47], are typically around 3025, 3000, 2950, 2930, 2910, 2890 and 2850 cm^{-1}. In our FTIR and FTR spectra we observed just three bands characteristic of PMMA sample around 3000, 2950 and 2846 cm^{-1}. This difference may be due to the strong overlapping bands character. The PED in this region reveals that (C—H) stretching modes are dominated by a combined stretching character between symmetric and asymmetric in αCH_3, OCH_3 and CH_2 groups. However, calculated frequencies at 3011 and 3000 cm^{-1} are pure modes with a very high contribution. Our calculations results in this region corroborate well with Refs. [46–48].

At 1730 cm^{-1}

The stretching carbonyl group shows a very intense mode in our IR spectrum and a medium mode at 1729 cm^{-1} in our Raman spectrum frequency. The PED assignments show that the stretching (C=O) is a pure mode with a high contribution (100%). This result is in agreement with previous theoretical and experimental works [31–36,45,47,49,54].

In the 1500–1300 cm^{-1} region

The region below 1500 cm^{-1} is the fingerprint of both infrared and Raman spectra. The spectra in this region are highly overlapped and mainly dominated by the symmetric and asymmetric vibrations (deformations in-plane bending, twisting, wagging, scissoring) of the ester methyl, α-methyl and methylene groups. A low skeletal (C—C) stretching vibration is also present. Our PED calculations show a mixed vibrational modes character between asymmetrical bending vibrations of α-methyl and ester methyl groups.

In 1300–950 cm^{-1} region

Despite the spectra of PMMA in this region have been analyzed by several earlier studies [31,52,56,59], the band assignments are not well addressed as reported in ref [60]. In addition, this region is very sensitive to the temperature, pressure, configuration and conformational changes [50,61]. However, the absorption bands in this region are known to be assigned to the asymmetric stretching of (C—C—O) mode coupled to the (C—O) stretching mode in the ester group [31,50,59]. This region exhibits two doublets bands corresponding to asymmetric stretching of (C—O); one calculated at (1150, 1189 cm^{-1}), observed at (1149, 1194 cm^{-1})$_{FTIR}$ and at (1145, 1182 cm^{-1})$_{FTR}$ and the second calculated at (1244, 1262 cm^{-1}), observed at (1242, 1273 cm^{-1})$_{FTIR}$ and at (1240, 1288 cm^{-1})$_{FTR}$. The splitting of these vibration frequencies is attributed to the rotational isomerism of the ester group [52]. Many authors [31,34,52] present these doublets as sensitive conformational doublets. However, (C—C) stretching vibrations modes calculated at (1064 cm^{-1}), observed at (1060 cm^{-1})$_{FTIR}$ and at (1064 cm^{-1})$_{FTR}$ seem to be insensitive to the conformation changes. This doublet is only present in syndiotactic PMMA [31,34]. The PED calculations of this region reveal that the majority of vibrational normal modes are strongly mixed between them with low contributions compared to other vibrational regions. This may be the main cause of the not well assignments definition in this region.

In the 950–250 cm^{-1} region

According to our theoretical results, the 900–250 cm^{-1} range cover mainly frequencies of complicated coupled vibrational modes, involving the deformation (rocking and in-plane bending) of CH_3 group, deformation (in-plane bending and out-of-plane bending) of (C=O) and (C—O) groups and stretching of (C—C) and (C—O) groups.

The 860 cm^{-1} vibrational mode, present in our calculated frequencies, seems to be almost dominated by the 841 cm^{-1} band in our FTIR spectrum (see Fig. 2). This indicates the lack of crystallinity in our syndiotactic PMMA polymer sample [58]. Vacatello and Flory [43] and Sundararajan [62] reported that isotactic PMMA does not absorb at 860 cm^{-1}. The PED indicates a strong mixing of the internal displacement coordinates with very low contribution to the energy potential distribution.

Table 3
PMMA Observed and calculated IR and Raman wavenumbers (in cm^{-1}), their assignments (symmetric, asymmetric, rocking, twisting, wagging, scissoring and bending) and their potential energy distribution, compared to other experimental and theoretical works.

Observed wavenumbers		Calculated Wave-numbers	Assignments	Assignments PED (%)	OTHER WORKS			
FTIR	FTR				FTIR Syn (Iso)	FTR Syn (Iso)	Theo.	Assignments (Exp/Theo)
–	–	3011	–	(100%) νasCTHC (OCH_3)	3026[f] (3029)[f] (3030)[i,j] (3025)[i] 3025[h,i]	3026[f] (3027)[f] 3013[d] (3027)[o] 3031[i]	3011[d] 3031[f]	Asym stretch OCH_3[d,f,h,i,j,o], sym stretch OCH_3[i]
3000 m	3000 m	3000	C—H asym stretching in OCH_3	(99%) νasCTHC (OCH_3)	2995[a,c,e,i] (2995)[c,i,r] 3000[d] 2998[j,k] (3000)[i,j] 2998[h,i] (3002)[i] 2996[g,i] (3004)[i]	3001[e] (3002)[e,i] (3006)[o] 2998[b] 3002[b] 3001[p] 3004[i] 3031[i]	3002[d,i]	Asym stretch OCH_3[a,b,c,d,e,g,h,i,j,o,p,r], asym stretch αCH_3[a,h,i,j,p], sym stretch αCH_3[i], sym stretch CH_2[c], asym stretch CH_2[i], out of plane OCH_3[i]
2950 vs	2953 vs	2958	C—H asym stretching in CH_2	(85%) νasC9HM + (13%) νasCTHC (OCH_3)	2948[a,c,e,i,r] (2948)[c,i] 2952[f,g,i,j] (2954)[f] 2953[d] (2953)[i,j] (2953)[i] 2958[i,k] (2958)[i] 2956[i] (2956)[i] 2957[h] 2962[s] 2960[s]	2953[d,e] (2953)[e,f] 2950[f,i] 2957[a,i] (2953)[o] 2954[b,i] 2957[p] 2960[i] 3002[i] 2955[i]	2951[d] 2952[f] 2957[i] 2950[i]	Sym stretch OCH_3[a,b,c,e,f,g,h,i,j,p,r], asym stretch αCH_3[c,f,h,i,j,o,s], sym stretch αCH_3[a,c,e,h,i,p], sym stretch CH_2[c,i], asym stretch CH_2[a,b,d,e,h,i,j,p], in plane OCH_3[i]
–	–	2925	C—H sym stretching in αCH_3	(80%) νsCTHC (αCH_3) + (18%) νsC9HM	2920[a,c,g,i] (2920)[c,e,i] 2929[f] (2914)[f] 2915[i] 2930[i,j] (2925)[i,j] (2930)[i] 2934[i] (2928)[i] 2928[i] 2915[i] 2925[k] 2933[h]	2932[e] (2932)[e] 2938[f] (2919)[f] 2920[a] 2920[b] 2939[j] 2928[i]	2931[f] 2938[i] 2920[i]	Asym stretch CH_2[f], sym stretch CH_2[a,b,e,h,i,j], sym stretch αCH_3[e,h,i,j], sym stretch OCH_3[a,b,i], asym stretch OCH_3[g,i]
–	–	2910	C—H sym stretching of OCH_3	(73%) νsCTHC (OCH_3) + (26%) νasC9HM	2915[a,k] (2910)[i] 2910[i] 2907[h]	(2919)[o] 2915[i]		Sym stretch OCH_3[a,h,i], sym stretch CH_2[a], asym stretch CH_2[o]
–	–	2889	C—H sym stretching of αCH_3	(57%) νsCTHC (αCH_3) + (39%) νsC9HM	2885[h,i,j] (2890)[i,j] 2890[i] 2895[k] 2892[h] 2883[s] 2882[s]	2893[f,i] 2890[i] 2880[i]	2892[f]	Sym stretch αCH_3[f,h,i,j,s], stretch OCH_3[h,i,j], asym stretch CH_2[s]
2850 w	2846 m	2858	C—H sym stretching in CH_2	(86%) νsC9HM + (12%) νsCTHC (OCH_3)	2835[c,e] (2835)[c] 2850[a,f,i] (2840)[f] 2840[d] 2844[g] 2845[i,j,k] (2842)[i,j] (2860)[i] 2860[i] 2855[h,i] (2845)[i] 2842[i] 2847[h] 2857[h] 2848[s]	2845[e,f,i] (2845)[e] (2842)[f] 2849[a] 2840[d] (2842)[o] 2864[b] 2848[p] 2857[i] 2847[i]	2851[f] 2835[d]	Sym stretch CH_2[f,o,s], stretching CH_2[h,i], def CH_2[i], sym stretch OCH_3[a,b,c,d,e,g,h,i,j,p], asym stretch OCH_3[i]·sym stretch αCH_3[h,i], in plane OCH_3[i]
1730 vs	1729 m	1730	C═O stretching	(100%) νCO	1730[a,c,e,i] 1740[f] 1731[f] (1736)[f] (1730)[c,i] 1727[d] (1750)[r] 1732[g] 1733[k] 1758[s]	1735[e] (1735)[e] 1731[f] (1738, 1725)[f] 1736[a,i] 1730[d] (1738, 1725)[o] 1724[b] 1736[p]	1732[f] 1724[d]	Stretch C═O[a,b,c,d,e,f,g,i,o,p,r,s], OCH_3 rocking[f], def CCO[o]
1485 m	1481 m	1488	In plane asym def of αCH_3	(53%) δasHCCTHC (αCH_3) + (42%) σHMC9HM	1483[a,c,d,e,g,h] (1483)[c] 1487[f] (1486)[f] 1483[j] (1483)[j] 1485[r] 1492[k]	1488[e] (1488)[e] 1487[d,f] (1486)[f] 1490[a] (1486)[o] 1483[i] 1480[i]	1478[f] 1480[d]	CH_2 sci[a,f], αCH_3 asym def[c,d,e,h,i,j,o,r], CH_2 bend[o]
1450 ms	1453 ms	1450	In plane asym def of OCH_3	(75%) δasHCCTHC (αCH_3) + (22%)δasHCCTHC (OCH_3)	1464[f,s] 1465[a,c,g,j] (1465)[c,j,l] (1450)[l] 1470[k] 1465[e] 1450[f,g,h,r] (1453)[f] 1452[a,c] 1452[j] (1452)[j] (1465)[r] 1455[k] 1460[h] (1445)[c] 1447[d]	1461[i] 1460[i] 1451[f,i] 1456[a] 1452[b] 1460[i,p] 1452[i] 1453[d,e] (1455)[e] (1447)[o]	1464[f] 1450[f]1446[d]	αCH_3 asym def [a,b,d,f,h,i,j,p,s], OCH_3 asym def[a,c,e,f,g,h,i,j,l,p,r,s], CH_2 bend[c,j,h,l,r], OCH_3 rocking[f], sym def OCH_3[c,o], rocking CH_2[e]
1434 ms	–	1437	In plane sym def of OCH_3	(65%) δsHCCTHC (OCH_3)	1445[e] 1436[f] (1442)[f] 1438[a,c,j,l,g,h,r] 1437[d] (1438)[j] 1442[k,s]	(1447)[f] (1432)[o] 1435[i] 1438[i]	1438[f] 1430[d]	OCH_3 sym def[a,c,d,e,f,l,r], OCH_3 bend[g,i,j,h], OCH_3 asym bend[o], OCH_3 rocking[o], bend CH_2[s]
–	1406 w	1402	CH_2 twisting	(61%) τωHMC9HM + (16%) ωHMC9CT + (16%) ωHCCTHC	1398[d] 1390[j] (1390)[j] 1391[k]	1400[a] 1388[o]	1388[d]	CH_2 twist or wag[a,h], CH_3 def[d], αCH_3 sym bend[j,o]

Table 3 (*Continued*)

Observed wavenumbers		Calculated Wave-numbers	Assignments	Assignments PED (%)	OTHER WORKS			
FTIR	FTR				FTIR Syn (Iso)	FTR Syn (Iso)	Theo.	Assignments (Exp/Theo)
1387 m	1383 w	1382	In plane sym def of αCH_3	(61%) δsHCCTHC (αCH_3)	1388[a,c,e,g,h,l,r] (1388)[c] 1382[f] (1386)[f] 1380[s]	1390[e,i] (1387)[d,e] 1389[f] (1388)[f]	1392[f] 1381[d]	αCH_3 sym, def[a,c,e,f,h,i,l,r,s], CH_2 def[d], OCH_3 bend[g]
1364 vw	1366 w	1363	CH_2 wagging	(50%) ωHMC9CT + (20%) νCTC9	1370[c,e,h,k] 1376[a] (1370)[c] 1367[d] 1370[l] (1370)[j] 1368[g] 1374[s] 1371[s]	1370[e] (1370)[e]	1364[d]	αCH_3 sym, def[a,c,s], twist or wag CH_2[e,j], CH_2 wag[d,s]
–	1324 w	1323	CH_2 wagging	(43%) ωHMC9CT + (31%) νC9CT + (13%) νCTCT + (10%) δSctcthc	1340[f] (1338)[f]	1325[e] 1326[f] (1335)[f] 1327[d] (1335)[o]	1335[f] 1320[d]	CH_2 wag[f,o], CH_2 twist[d], CC stretching[o], αCH_3 sym bend[o]
–	–	1310	CH_2 wagging	(33%) ωHMC9CT + (24%) νCTC + (17%) νC9CT	1316[f] 1303[s]		1310[f]	CC stretch[f], CH_2 wag[f], CH_2 twist[s]
1273 vw	1288 w	1262	Asym stretching of (C—O)	(50%) νasCOE + (29%) νasOECT + (12%) νCTC	1295[e] (1295)[c] 1278[f] (1268)[i] 1270[a,c,g,l,r] (1260)[c,r] 1267[d] 1268[n] (1260)[l] 1276[k] 1273[m] (1265)[m]	1272[e] (1281)[e] (1270)[f] 1276[a] (1270)[o] 1336[b] 1264[p]	1271[f] 1261[d]	CC stretch[f,o], asym stretch CCO[a,b,c,l,n,p,r], stretch CO[a,b,c,d,n,p,r], asym stretch COC[e,l], CH_2 twist[o], CC bend[o], CCC def[o], αCH_3 sym def[l,r]
1242 m	1240 w	1244	Asym stretching of (C—O)	(58%) νasCOE + (22%) νasOECT	1252[e] 1242[f,g,m] 1240[a,c,l] (1252)[c,l,r] 1239[d,m] 1238[n] 1240[r] (1239)[l] 1248[k] 1251[s]	1238[e] 1241[f] (1231)[f] 1234[a] 1240[d] (1231)[o] 1238[b]	1241[f] 1238[d]	CO stretch[b,c,d,f,l,n,o,r,s], CC stretch[f,r], asym stretch CCO[a,b,c,l,n,r], asym stretch COC[e], CH_2 twist[o], CO in plane bend[o], band associated with vibrations of ester groups of PMMA[g]
1194 m	1182 w	1189	Asym stretching of (C—O—C)	(55%) νasOECT + (17%) νasCOE + (15%) δOECTHC	1190[a,c,e,r] 1193[f,m] 1197[d,s] (1198)[f] (1190)[c,r] 1192[n] (1191)[l] 1191[l] 1194[g] 1200[k] (1195)[m]	1188[a,e] (1190)[e] 1183[f] 1187[d] (1190)[o]	1191[f] 1190[d]	OCH_3 rock[f,s,o], OCH_3, asym bend[f], CH_2 twist[f,o], skeletal stretching coupled with internal CH def vibration[c,n,r], asym stretch COC[a,e,l], CH_3 wag[d], CH_2 wag[o], band associated with vibrations of ester groups of PMMA[g]
1149 ms	1145 w	1150	Asym stretching of (C—O—C)	(44%) νasOECT + (22%) νasCOE + (15%) δOECTHC	1150[a,c,e,g,r] 1149[f,l,m] (1150)[c,r] 1147[d] 1148[n] (1147)[l,m] 1155[k]	1160[d,e] (1152)[e] 1158[f] 1161[a] (1157)[o] (1150)[o]	1156[f] 1155[d] 1138[d]	CC stretch[f,l,o], skeletal stretching coupled with internal C—H def vibration[c,n,r], asym stretch COC[a,e,l,o], CH_3 wag (CH_3 twist)[d], CH_2 wag[o], α-CH_3 rock[o], CH_2 twist[o]
–	1124 w	1110	Stretching of (C—C)	(29%) νCTCT + (16%) νCTC9 + (14%) δOECTHC + (10%) δCTCTHC	1122[e,f,s] (1115)[f] 1125[n] (1104)[l] 1161[l] 1099[s]	1123[e] (1120)[e] 1126[f] (1123)[f] 1125[a] 1127[d] (1123)[o] (1113)[o]	1118[f] 1121[d]	OCH_3 rock[f,o], OCH_3 asym bend[f,o], backbone stretch CC[a,e,l,n,s], CH_3 wag[d]
1060 w	1064 w	1064	C—C Stretching	(46%) νCTCT + (25%) νCTC9 + (15%) δOECTHC	1065[f] 1063[a,c,g] 1060[n] 1068[k] 1057[s]	1063[e] (1050)[e] 1064[f] (996)[f] 1067[d] 1062[b] 1081[p]	1068[f] 1064[d]	OC stretch[f], OCH_3 rock[f,s], band arises from intramolecular interaction[c,n], backbone stretch CC[a,b,e,g,p], CH_3 twist[d]
–	1044 vw	1046	CH_3 twisting and C—C stretching	(33%) τωHCCTC9 + (31%) νCTC9 + (13%) τωCTCTHC	1050[d]	1046[d]	1042[d]	CH_3 twist[d]
–	–	1023	OCH_3 rocking	(45%) ρOECTHC + (31%) νCOE + (15%) δHCCTHC	1026[f] (998)[f] 1038[s]	1027[d]	1022[d]	OC stretch[f], OCH_3 rock[f], CC stretch[d], CH_2 rock[s]
989 m	989 m	980	C—O stretching and In plane bending of OCH_3	(25%) νaCOE + (21%) νCTCT + (20%) δOECTHC + (11%) νCTC9 + (10%) νaOECT + (10%) νCTC	989[t] 996[e] 992[f] (996)[c] 990[d,g] 988[a,c,r] 996[k] (996)[r] (995)[t]	(995)[e] 990[d] (996)[o] 988[e] 987[f] (996)[f] 991[a] 988[b] 999[p]	991[f] 981[d] 985[f]	αCH_3 rock[f], OC, stretch[f,o], asym stretch COC[c,g], rock OCH_3[a,b,c,e,g,o,p,r], CC stretch[d]

966 w	965 m	957	OCH_3 rocking	(32%) ρCTCTHC (αCH_3) + (22%) ρHMC9CT + (17%) νCTC + (15%) νCTCT + (10%) νCOE	951[e,f] (951)[c,f] 967[a,c,d,f,g,r,t] (950)[r] 972[k] 968[s] 946[s] (953)[t]	967[e,f] (953)[e,f] (960)[f] 970[a,d] (960)[o] (953)[o]	935[f] 980[f] 968[d]	αCH_3 rock[a,c,e,f,g,o,r,s], CH_2 rock[f,o], CC stretch[d,f,o]
912 vw	–	913	CH_3 rocking and CH_2 rocking	(33%) ρCTCTHC (αCH_3) + (27%) ρHMC9CT	913[d,f] 910[a,c,t] 915[g] 916[k]	912[e] 915[f] 920[d] 914[b] 925[p]	915[f] 905[d]	CH_2 rock[b,f,p], CH_3 rock[d]
860 vw	–	860	CH_3 rocking and CH_2 rocking	(36%) ρCTCTHC + (30%) ρHMC9CT + (14%) νC9CT + (12%) νCTCT	863[f] 860[t]	877[e] 876[f] 878[b] 880[d]	881[f] 868[d]	CC stretch[f], CH_2 Rock[b,f,t], CO stretch[f] CH_3 rock[d]
841 w	837 w	839	CH_2 rocking	(30%) ρHMC9CT + (26%) ρCTCTHC + (16%) νCOE + (13%) νC9CT + (11%) νCTCT	842[a,c,e,g] (842)[c] 840[d] 830[k] (843)[f] 845[k] 844[s] 841[t]	842[e] (841)[e] 833[a] 840[d] (844)[f,o]	828[d]	CC stretch[f,o,s], CH_2 rock[a,b,d,e,g,f,o,t], CO stretch[f,o]
808 vw	813 s	796	C—O sym stretching	(24%) νsOECT + (21%) νsCOE + (19%) νCTCT + (10%) ρHMC9CT	810[e,f,g] (808)[f] 807[a,c,d,q] (810)[c] 786[q] 827[g] 812[k]	815[e] (809)[e,f] 812[f] 796[a] 810[d] (809)[o] 818[a] 812[b] 786[q]	800[f] 805[d] 803[q] 796[q]	CO stretch[f,]CC stretch[f,o,q], sym stretch COC[a,b,e,g,o], C═O in plane bend[f]
750 m	–	767	C═O out of plane bending	(64%) γC O + (16%) νCOE + (15%) δOCOE	759[e] 747[f] (764)[f] 749[a,r,t] (759)[c,r,t] 752[g]	767[e] (774)[e] 736[a] 733[d] (782)[o] (764)[o] 732[b] 853[p]	755[f] 725[d] 761[q]	C═O out of plane bend[d,f,o], rock CH_2[c], stretch CC skeletal mode[a,b,c,g,p,r], CO in plane bend[d], C bend[o,r]
–	–	742	C═O out of plane bending	(42%) γC O + (13%) νCOE + (13%) δOCOE + (10%) νCTCT + (10%) νC9CT + (10%) νCTC	749[c] 750[d,s] 749[q] 753[k]	(742)[e] 732[q]	739[d] 761[q]	Rock CH_2[c,s], stretch CC[c,e,q], C═O out of plane bend[d]
–	600 m	607	In-plane bending (C—C═O)	(44%) δCTCO + (30%) νCTCT	643[f] 598[a,f] (609)[f]	601[e] 602[f] (597, 562)[f] 604[a] 600[d] 600[b] (597)[o] 602[p]	660[f] 595[d]	CCOO stretch[a,b,f,o,p], CO in plane bend[d,f,o], sym bend CCO[a,e,b,p]
590 w	559 w	570	In plane bending of (C—C═O)	(32%) δCTCO + (26%) δC9CTCT + (24%) νCTCT + (15%) νCTC	560[e] (559)[f,i] 552[a] (560)[c] 554[c] 552[q] (568)[i]	555[e] (561)[e] 537[a] 560[d] (562)[o] 558[b] 552[q]	550[d] 591[q]	Def CCC[a,b,e,i], CC in plane bend[d], CC stretch[i,o,q], CO in plane bend[o], wag of αCH_3[i]
–	526 vw	501	In plane bending of (C—C—O)	(35%) δCOECT + (30%) νCTCT	508[f] 505[a] 510[c,k]	509[n] 504[a] 513[d]	502[d]	CCO def[n], CC bend[d,n], in plane asym def CCO or C═O in plane def[a]
482 vw	485 vw	482	In plane bending of C—C—O)	(27%) δCOECT + (25%) δCTC9CT + (17%) δCTCOE + (13%) δCTCTCT	486[f] (480)[f,i] 484[a,c,e,g] 485[k]	484[e,f] (480)[e] (481)[f] 487[a,d] (481)[o]	484[f] 478[d]	CCO def[c,f,o], CC bend[d,f,i,o], Out of plane def CCO[a,e,g], CCC def[o,i]
–	454 vw	459	In plane bending of (O—C═O)	(25%) δCTCO + (23%) γCOE + (20%) δCTCOE + (10%) δC9CTCT + (10%) δCTCTC	459[f] (476)[f]	(464)[f] (464)[o]		CCO def[f,o], CCC def[f,o], C bend[o]

Table 3 (*Continued*)

Observed wavenumbers		Calculated Wave-numbers	Assignments	Assignments PED (%)	OTHER WORKS			
FTIR	FTR				FTIR Syn (Iso)	FTR Syn (Iso)	Theo.	Assignments (Exp/Theo)
–	391 vw	390	In plane bending of (C—O—C)	(40%) δCOECT + (16%) δCTCTCT + (14%) δCCTCT + (13%) δCTC9CT	400[a] (391)[i] 420[k]	391[f] 400[a] (390)[o]	392[f]	Def COC[a] C bend[o], CCC def [o], wag of αCH_3[i]
–	365 w	365	In plane bending of (C—O—C)	(35%) δCOECT + (32%) δCTC9CT + (17%) δCTCTCT + (14%) δCTCTC	364[f] (365)[f] 360[a]	366[e] (373)[e] 363[f] (372)[f] 370[a] 367[d] (372)[o] (341)[o]	360[f] 361[d]	CCC def[f,o], COC def[f,o], in plane sym bend CCO[a,e, o], CO out of plane bend[d]
–	–	327	In plane bending of (C—C—C)	(33%) δC9CTCT + (32%) δCOECT	320[a] 320[q]	304[a] (314)[o] 296[q]	370[q]	Def CCC[a,o, q], C bend[o]
–	299 w	283	In plane bending of (C—C—C)	(25%) δC9CTC + (20%) δCOECT + (15%) δCTCTC9		301[f,e] 300[d]	295[f] 291[d]	CO out of plane bend[d]
–	252 vw	260	In plane bending of (C—C—C)	(25%) δC9CTC + (20%) δCOECT + (16%) τOECT + (15%) δCTCTC9	319[f] 276[f] (314)[f] 295[a]	275[f] (314)[f] 267[d]	284[f] 250[d]	CO in plane bend[f], CCC def[f], CC bend[d,f]
–	–	203	Torsion of (C—O)	(55%) τOECT	216[q] 225[q] (188)[i]	200[d] (221)[o] 216[q]	192[d] 201[q] 182[q]	CC out of plane bend[d,q], CO torsion[o], CCC bend[o,q], def OCH_3[i]
–	–	189	Torsion of (C—O)	(40%) τCOE + (28%) τOECT + (15%) δC9CTC		163[d]	169[d]	CC out of plane bend[d]
–	–	146	Torsion of (C—C)	(60%) τCTC9		153[f] 140[d]	170[f] 144[d]	CC torsion[d]
–	–	116	Torsion of (C—O)	(72%) τCOE + (22%) τCTC	(113)[i] (109)[i]			CO torsion[i]
–	–	87	Torsion of (C—O)	(78%) τCOE + (20%) τCTC	95[q]	(85)[o]	73[q]	CC stretch[o], C bend[o], CCC def[o] Out of plane bend of CCC[q], CO torsion[i]
–	–	62	Torsion of (C—O)	(81%) τCOE	58[q]			Hindered rotation or translation[q]

Note 1: αCH_3 is the methyl group and OCH_3 is the ester methyl group.
Note 2: vs: very strong; s: strong; ms: medium strong; m: medium; w: weak; vw: very weak;
ν: stretching; δ: in plane bending; γ: out of plane bending; τ: torsion; ρ, rocking; *νs*:, symmetric stretching;
νas: asymmetric stretching; δs: symmetric deformation; δas: asymmetric deformation; τω: twisting; ω: wagging σ: scissoring.

[a] Ref. [31].
[b] Ref. [33].
[c] Ref. [34].
[d] Ref. [35].
[e] Ref. [36].
[f] Ref. [44].
[g] Ref. [45].
[h] Ref. [46].
[i] Ref. [47].
[j] Ref. [48].
[k] Ref. [49].
[l] Ref. [50].
[m] Ref. [51].
[n] Ref. [52].
[o] Ref. [53].
[p] Ref. [54].
[q] Ref. [55].
[r] Ref. [56].
[s] Ref. [57].
[t] Ref. [58].

Below 250 cm^{-1}

Few bands are observed and calculated below 250 cm^{-1}. The C—O and C—C torsional vibrations were expected. The PED indicates large coupled contributions between these torsional vibrations.

4.4. The accuracy and transferability of the SPASIBA parameters

The accuracy of a molecular mechanics force field is related to its force parameters transferability from one molecule to another. Good parameters should generally be able to reproduce various physical properties of different molecular systems with same chemical structures.

The aim of this subsection is to check the transferability of SPASIBA force constants (developed for PMMA) to PMA, PMAA and PAA polymers. To this end, we have analyzed the normal modes of these polymers by means of the same PMMA calculations method and same number of monomer units. Most of the PMMA force field refined parameters are used to establish the vibrational wavenumbers of the others studied polymers, with additional force constant namely (HE—OE) bonding energetic terms present on the PMAA and PAA structures, (C—CT—HC) for PMAA and (C—OE—HE) for PAA valence angle energetic terms (see Table 1(a) and (b)).

Optimized geometrical parameters of our PMA, PMAA and PAA polymers are summarized in Table 4(a)–(c). The bond lengths and valence angles average deviations relatively to literature values given in Table 4(a)–(c) are (0.037 Å, 2.2°)$_{PMA}$, (0.020 Å, 5.4°)$_{PMAA}$ and (0.037 Å, 3.1°)$_{PAA}$.

The discrepancies observed in angles values between our results and literature values are mainly due to the difference between the models used for comparison (copolymers against our homopolymers of 100 monomers). We note here, that our PMA, PMAA and PAA polymers exhibit each the same 10/1 helix conformation with *tt* sequence deduced above for our PMMA polymer.

In Table 5 we summarize the calculated vibrational wavenumbers and their PED attributions of PMA, PMAA and PAA along with our PMMA and previous experimental results.

As it can be noticed from Table 5, all studied acrylic polymers present almost same symmetrical and asymmetrical stretching vibrational normal modes of CH_3 and CH_2 groups in the mid-infrared region with high PED contribution. These results agree well with experimental vibrational bands in the FTIR or FTR spectrum of the acrylic polymers reported in the literature for PMA [57,66], PMAA [57,67,68] and PAA [68–70].

The calculated (C=O) stretching frequencies at 1730 cm^{-1} (for PMMA, PMA and PAA) and at 1732 cm^{-1} for PMAA were already reported in previous experimental results in 1700–1750 cm^{-1} region [66–71]. We note also that the symmetrical and asymmetrical of CH_3 and CH_2 deformation vibrations in the [1500–1430] cm^{-1} region were observed by many authors for some Acrylic polymers [57,66–70].

Below 1430 cm^{-1}, and at the same wavenumber, the PED calculations give different assignments for the studied polymers. As it can be observed from Table 5, PAA and PMAA exhibit same (C—O) stretching coupled with (O—H) in-plane bending attributions, whereas, PMMA and PMA present asymmetrical deformation of ester methyl group. These dissimilarities in mode attributions are due to the sensitivity of the SPASIBA force field to the atomic positions in the chemical structure and were already reported in many previous experimental results [48,66,67,70]. The PED calculations show the presence of the hydroxyl stretching vibration of (O—H) group around 3447 cm^{-1} and 3441 cm^{-1} for PMAA and PAA, respectively. These (O—H) stretching vibrations are pure modes with high contributions to the potential energy distribution. From vibrational wavenumbers and their assignments of the studied

Table 4
Mean value geometrical parameters of PMA, PMAA and PAA optimized by SPASIBA force field along with other experimental and theoretical results. Bonds are given in Å and valence and dihedral angles in degrees.

(a) Optimized geometrical parameters of PMA

Parameters	Our results	Other works [63]
CT—HC	1.110	1.069, 1.070, 1.076, 1.080
C—OE	1.352	1.352, 1.350
C=O	1.203	1.206, 1.207
CT—OE	1.430	1.452
CT—C	1.530	1.473, 1.474
CT—C9	1.560	1.316
C9—HM	1.107	1.072, 1.073
HC—CT—HC	108.81	109.0, 110
OE—CT—HC	109.49	105, 110
CT—C—OE	113.13	111, 113
O=C—CT	123.61	125, 126
C9—CT—HC	110.93	124
C—CT—C9	112.78	120, 123
CT—C9—HM	108.69	121, 122
HM—C9—HM	105.51	117
O=C—OE	124.02	122, 123
HC—CT—C	111.66	114, 116
C9—CT—C9	111.80	–
CT—C9—CT	119.01	–
X—CT—C9—X	−26.44, 17.13	–
X—CT—C—X	−7.01, 179.03	–

(b) Optimized geometrical parameters of PMAA

Parameters	Our results	Other works
CT—HC	1.102	–
CT—CT	1.542	–
C=O	1.200	1.234[a], 1.230[b]
C—OE	1.352	1.368[b]
CT—C	1.542	–
CT—C9	1.573	–
C9—HM	1.101	–
HE—OE	0.960	0.971[a], 0.967[b]
CT—C9—HM	102.35	–
C—CT—C9	111.14	–
O=C—CT	128.26	–
C—OE—HE	105.06	109.97[a]
HM—C9—HM	106.05	–
HC—CT—HC	107.65	–
O=C—OE	119.10	113.22[b]
CT—CT—C9	110.77	–
CT—C9—CT	127.45	–
CT—CT—HC	111.12	–
CT—CT—C	111.44	–
C9—CT—C9	102.41	–
X—CT—C9—X	−20.84, 22.71	–
X—CT—C—X	−11.78, 178.32	–

(c) Optimized geometrical parameters of PAA

Parameters	Our results	Other works [63]
CT—HC	1.110	1.069, 1.070, 1.072
C—OE	1.360	1.356, 1.357, 1.358, 1.359
C=O	1.199	1.199, 1.204, 1.205
CT—C	1.540	1.470, 1.471, 1.485, 1.487
CT—C9	1.567	1.306, 1.315, 1.316
C9—HM	1.109	1.072
HE—OE	0.965	0.961, 0.963, 0.968
CT—C9—HM	109.91	120, 121, 122, 124
HM—C9—HM	104.78	117, 118
C9—CT—HC	105.62	121, 122, 123, 124
C—CT—C9	114.02	120, 123, 126
O=C—CT	127.30	122, 124, 125, 127
C—OE—CT	113.87	111, 113, 116, 118
C—OE—HE	108.68	112, 115, 117
O=C—OE	118.95	120, 122
CT—C9—CT	119.77	–
HC—CT—C	101.10	114, 116, 118
C9—CT—C9	113.36	–
X—CT—C9—X	−26.18, 16.82	–
X—CT—C—X	6.56, 174.39	–

[a] Ref. [64].
[b] Ref. [65].

Table 5
Calculated wavenumbers and PED of PMA, PMAA and PAA obtained using the optimized force constants from the empirical SPASIBA force field (PMMA wavenumbers values and attributions are reproduced here for more clarity).

Calculated wavenumbers (cm^{-1})				PED % assignments				Other works					
PMMA	PMA	PMAA	PAA	PMMA	PMA	PMAA	PAA	PMA		PMAA		PAA	
								FTIR/FTR	Assignments	FTIR/FTR	Assignments	FTIR/FTR	Assignments
–	–	3447	3441	–	–	(98%) νOEHE	(98%) νOEHE			(3572–3540)[a,g]	O—H stretch[a,g]	3100–3200 [i]	OH stretch[i]
3000	3075	3006	3076	(99%) νasCTHC (OCH_3)	(97%) νasCTHC	(83%) νasCTHC	(100%) νasCTHC	2998[b]	CH_3 asym stretch[b]	3001[g]	CH_2 stretch[g]		
2958	2964	2962	2967	(85%)νasC9HM + (13%) νas CTHC (OCH_3)	(63%) νasC9HM	(63%) νasC9HM	(63%) νasC9HM	2970[b]	Stretch CH[b]	(2960–2971)[a,g]	CH_3 asym stretch[a,g]		
–	2943	2941	2942	–	(41%)νsCTHC + (27%)νasC9HM	(40%) νsCTHC + (27%) νasC9HM	(43%) νasC9HM + (24%) νScthc	2959[b]	Sym stretch CH_3[b]	2939[g]	CH_3 sym stretch[g]		
2925	2930	2930	2929	(80%) νsCTHC(αCH_3) + (18%) νsC9HM	(68%) νasC9HM	(61%) νasC9HM	(67%) νasC9HM	2924[b]	CH_2 asym stretch[b]	2928[a]	CH_2 asym stretch[a]	(2877–2930)[i,f]	CH_2 or CH stretch[f] CH_2 asym stretch [i]
2889	2885	2883	2882	(57%) νsCTHC (αCH_3) + (39%) νsC9HM	(52%) νsC9HM + (43%) νsCTHC	(53%) νsCTHC + (45%) νsC9HM	(55%) νsC9HM + (41%) νsCTHC	2883[a]	CH_2 asym stretch[a]	2882[a]	CH_3 sym stretch[a]		
2858	2845	2842	2845	(86%) νsC9HM + (12%) νsCTHC (OCH_3)	(85%) νsC9HM	(83%) νsC9HM	(85%) νsC9HM	2847[b] 2848[a]	CH_2 sym stretch[a,b]	2839[a]	CH_2 sym stretch[a]	2860[i]	CH_2 stretch sym[i]
1730	1731	1734	1731	(100%) νCO	(99%) νCO	(99%) νCO	(95%) νCO	1733[b] 1758[a]	νC═O[a,b]	(1673–1767)[a,c,d,g,h]	C═O stretch[a,g,d,h] COO[c]	(1686–1742)[d,e,f,i]	C═O stretch [d,e,f,i]
1488	1485	1483	1485	(53%) δasHCCTHC (αCH_3) + (42%) σHMC9HM	(38%) δasHCCTHC + (24%) δasOECTHC + (18%) νOECT	(60%) δasHCCTHC + (26%) νOEHE	(54%) δasHCCTHC + (25%) νOEHE			1487[c] 1483[d]	OH[c], CH_3 def[d]		
1450	1450	1450	1453	(75%) δasHCCTHC (αCH_3) + (22%) δasHCCTHC (OCH_3)	(71%) δasHCCTHC + (10%) δHMC9HM	(49%) δHMC9HM + (16%) δasHCCTHC	(62%) δHMC9HM + (13%) δCTCTHC	1452[b] 1442[a]	CH_3 asym def[b] CH_2 bend[a]	(1448–1455)[c,d,g] 1455[a]	CH_3 asym, def[g], CH_2[c], CH_2 def[a,d]	(1451–1460)[d,e,f,i]	CH_2, def [e,i] CH_2 def[d,f]
1437	1434	1432	1434	(65%) δsHCCTHC (OCH_3)	(64%) δasHCCTHC + (19%) δHMC9HM	(64%) δasHCCTHC + (35%) COEHE	(72%) δasHCCTHC + (31%) COEHE	1434[b]	CH_3 sym def[b], CH_2 def[b]	1432[h]	O–H/acid carboxyl stretch[h]		
–	1416	1424	1419	–	(55%) δasHCCTHC	(52%) νCOE + (23%) δCOEHE + (10%) νC9CT	(44%) νCOE + (33%) δCOEHE + (10%) νCTC			1415[c] 1413[c]	COO[c]	(1413–1415)[d,f,i]	CO stretch[d,f], OH def[d,f], CH_2 bend[i]
1402	1403	1401	1397	(61%) τωHMC9HM + (16%) ωHMC9CT + (16%) ωHCCTHC	(31%) τωHMC9HM + (23%) δsHCCTHC + (14%) ωCTC9HM + (13%) ωHCCTCT	(45%) νCOE + (39%) δCOEHE	(43%) νCOE + (38%) δCOEHE			1389[c] 1390[d]	COO[c], CO stretch[d], OH def[d]	1402[d] 1400[i]	COO sym stretch[d], [i], OH in plane bend[i]
1363	1369	1371	1379	(50%) ωHMC9CT + (20%) νCTC9	(43%) ωHMC9CT + (21%) δHCCTC9	(30%) δsHCCTCT + (12%)νCOE + (12%) νC9CT	(29%) δsHCCTCT + (23%) δHCCTC9	(1374–1180)[a,b]	CH_3 wag[b], CH_2 wag[a]	(1371–1381)[a,d,g]	CH_3 sym def[a,g]		
1323	1346	1331	1333	(43%) ωHMC9CT + (31%) νC9CT + (13%) νCTCT + (10%) δsCTCTHC	(34%) δsHCCTHC + (23%) δHCCTC9 + (15%) δHMC9HM	(30%) ωHMC9CT + (12%) δCTCTC	(41%) ωCTC9HM + (16%) δHCCTC + (14%) δC9CTHC	1330[b]	CH def[b]	1354[g] 1324[c]	C–O–H bend[g] CH_2[c]	1320–1345[d,e,f]	CH_2wag[d], CH def[d], CH_2 twist[e,f]
1310	1302	1280	1295	(33%) ωHMC9CT + (24%) νCCT + (17%) νC9CT	(38%) ωCTC9HM + (17%) νCTC + (14%) νCOE + (10%) δHCCTC	(29%) ωCTC9HM + (24%) νCTC9 + (15%) νCTCT + (14%) νCTC	(49%) ωHMC9CT + (12%) νCTC	1302[a] 1175–1302[a]	CH_2 twist[a]	(1280–1304)[a]	CH_2 wag[a]		
1262	1267	1258	1276	(50%) νasCOE + (29%) νasOECT + (12%) νCTC	(55%) νasCOE + (21%) νasOECT + (12%) νCTC + (10%) δCTC9HM	(48%) δCOEHE + (24%) νCOE	(56%) δCOEHE + (30%) νCOE	1260[b]	CCOO stretch[b], skeletal stretch[b]	1262[a,d]	CO stretch[a], OH def[d]		
1244	1256	1243	1255	(58%) νasCOE + (22%) νasOECT	(45%) νasCOE + (16%) νCTC + (14%) νOECT	(53%) δCOEHE + (18%) νCOE	(53%) δCOEHE + (26%) νCOE	1251[a]	C—O stretch[a]	1197–1245[a]	CH_2 twist[a]	1247[d] 1248[f]	CO stretch[d], OH def[d], C—O stretch coupled with O—H in-plane bend[f]
1189	1167	1179	1174	(55%) νasOECT + (17%) νasCOE + (15%) δOECTHC	(34%) νOECT + (16%) νC9CT + (13%) νCOE + (10%) δCOEHC	(69%) δCOEHE + (25%) νCOE	(28%) δCOEHE + (22%) νCTC9 + (20%) νCOE	(1161–1175)[a,b]	CCOO stretch[b], skeletal stretch[a,b], CH_2 twist[a]	(1171–1176)[a,c,d]	COOH[c,d] C—C stretch[a]	1170[d]	COOH[d]

1150	1131	1122	1131	(44%) νasOECT + (22%) νasCOE + (15%) δOECTHC	(47%) νOECT + (19%) νCTC9 + (13%) δCTCTHC	(58%) νCOE + (27%) δCOEHE	(32%) νCOE + (29%) δCOEHE + (14%) δHCCTC9	1120[b]	C—C stretch[b]	(1066–1122)[a,g]	C–O stretch[g] αCH_3 stretch[a]	1130[i]	CH bend[i]
1046	1051	1052	–	(33%) τωHCCTC9 + (31%) νCTC9 + (13%) τωCTCTHC	(41%) ρHMC9HM + (27%) νCTC + (15%) νCTC9	(43%) ρHMC9HM + (14%) νCTC9 + (12%) δCCT	–	1050[b] (721–1038)[a,b]	C—C stretch[b] CH_2 rock[a]	1010–1057[a]	CH_3 rock[a]	1026[f]	CH_2 rock[f]
957	956	949	940	(32%) ρCTCTHC (αCH_3) + (22%) ρHMC9CT + (17%) νCTC + (15%) νCTCT + (10%) νCOE	(37%) ρHCCTHC + (20%) ρHMC9CT + (10%) νCTC	(43%) γOE HE + + (22%) δHCCTC9	(39%) γOE HE + (22%) δHCCTC9	956[b]	CH_3 rock[b]	(933–950)[a,c,g]	CH_2 wag[g], αCH_3[c], OH out of plane bend[a]	945[i]	OH bend[i]
839	848	855	842	(30%) ρHMC9CT + (26%) ρCTCTHC + (16%) νCOE + (13%) νC9CT + (11%) νCTCT	(46%) νCTC + (18%) ρCTC9HM	(49%) νCTCT + (29%) δCTC9HM + (18%) δHCCTC9	(22%) νCTC + (14%) δCTC9HM	844[a]	C—COO stretch[a]	857[c]	CCH_3[c]	(830–846)[e,f,i]	C—COOH stretch[e,f], CH bend[i]
796	824	799	812	(24%) νsOECT + (21%) νsCOE + (19%) νCTCT + (10%) ρHMC9CT	(32%) ρCTCTHC + (24%) ρCTC9HM + (15%) νC9CT	(47%) νCTC + (15%) τωHMC9CT	(35%) νCTC + (28%) τωCTC9HM	825[b]	CH_3 rock[b]	800[a,c]	C—COOH[a,c], CC stretch[c]	(800–804)[e,f,i]	C—COO stretch[e,i], CH_2 twist and CH bend[i]
742	744	730	745	(42%) γC O + (13%) νCOE + (13%) δOCOE + (10%) νCTCT + (10%) νC9CT + (10%) νCTC	(44%) ρCTC9HM + (32%) γC O + (11%) νCOE + (11%) δOCOE	(50%) δCTC9CT + (12%) δOCOE	(55%) δCTC9CT + (23%) δOCOE	721[a] 755[b]	CH_2 rock[a,b]	721[c]	CCC skeletal def[c] (COH)	745[i]	CH bend[i]
–	631	636	630	–	(44%) γC O + (30%) δCTCO + (10%) νCTCT	(28%) δCTC9CT + (22%) δOCOE	(36%) δOCOE + (26%) δCTC9CT + (20%) δCTCO	625[b]	CH_3OCO out-of-plane bend[b]	(631–642)[c,g]	C–H vinyl wag[g] CCC skeletal def[c] (COH)		
607	608	593	584	(44%) δCOECT + (30%) νCTCT	(51%) γC O + (25%) δCTCO + (10%) νCTCT	(55%) γC O + (33%) δCTCO + (10%) νCTCT	(53%) γC O + (29%) δCTCO + (11%) νCTCT	584[a]	C═O out of plane bend[a]	595[c] 584[a]	CCC skeletal def[c] C═O out of plane bend[a]		
501	511	511	512	(35%) δCOECT + (30%) νCTCT	(23%) δCOECT + (15%) δOCOE + (13%) δC9CTCT + (12%) νCTCT	(37%) δCTCO + (15%) ωCTCOE + (13%) δCTCTC	(17%) δCTCOE + (13%) δCCTCT + (12%) νCTCT	565[b]	CCO in-plane bend[b]	512–533[c]	CCC skeletal def[c]		
365	367	362	365	(35%) δCOECT + (32%) δCTC9CT + (17%) δCTCTCT + (14%) δCTCTC	(47%) δCOECT + (29%) δCCTCT + (10%) νCTC	(46%) δCOECT + (23%) δCTCTC9	(49%) δCTCOE + (12%) δC9CTC9 + (12%) νC9CT	470 –480[b]	COC in-plane bend[b]	358[h]	C–C–C bend/twist[h]		
–	–	341	348	–	–	(55%) τCOE + (32%) δC9CTCT + (11%) δCTCOE	(54%) τCOE + (14%) δC9CTC + (11%) δCTCO + (10%) δC9CTCT	345[b]	COC out-of-plane torsion[b]	343[c]	CCC skeletal def[c]		

Note 1: αCH_3 is the methyl group and OCH_3 is the ester methyl group.
Note 2: ν: stretching; δ: in plane bending; γ: out of plane bending; τ: torsion; ρ, rocking; ν s:, symmetric stretching.
νas: asymmetric stretching; δs: symmetric deformation; δas: asymmetric deformation; τω: twisting; ω: wagging σ: scissoring.

[a] Ref. [57].
[b] Ref. [66].
[c] Ref. [67].
[d] Ref. [68].
[e] Ref. [69].
[f] Ref. [70].
[g] Ref. [71].
[h] Ref. [72].
[i] Ref. [73].

polymers we can state that the principle of transferability proposed by Shimanouchi [18,74] is confirmed.

5. Conclusion

In the present study, we carried out a complete vibrational assignments and analysis of acrylic polymers using SPASIBA force field. The results of normal coordinate analysis have been discussed and compared to previous theoretical and experimental works. We were able to reproduce all fundamental vibrational modes and their assignments observed in FTIR and FTR spectra. The principle of transferability established by Shimanouchi has been also validated. Consequently, the parameters of the SPASIBA force field obtained from our study might be useful for further vibrational normal mode calculations of molecules containing the same chemical subgroups as our acrylic polymers.

References

[1] R. Sinha, Outlines of Polymer Technology, Prentice-Hall by India Private Ltd., New Delhi, 2002.
[2] A. Soldera, N. Metatla, Compos. A: Appl. Sci. Manuf. 36 (2005) 521.
[3] F. La Mantia (Ed.), Handbook of Plastics Recycling, 1st ed., Rapra Technology Ltd., Shropshie, 2002.
[4] J.A. Brydson, Plastics Materials, 6th ed., Butterworth-Heinemann, Oxford, 1995, pp. 411.
[5] S. Saha, S. Pal, J. Biomech. 17 (7) (1984) 467–478.
[6] B. Kaczmarczyk, B. Morejko-Buz, A. Stolarzewicz, Fresenius J. Anal. Chem. 370 (2001) 899–903.
[7] M. Sevegney, R. Kankan, A. Siedle, R. Naik, V. Naik, Vib. Spectrosc. 40 (2006) 246–256.
[8] F.J. Boerio, J.L. Koenig, J. Macromol. Sci. C7 (1972) 209.
[9] G. Zifferer, A. Kornherr, J. Chem. Phys. 122 (2005) 204906.
[10] K. Tasaki, Macromolecules 29 (1996) 8922.
[11] J. Ennari, J. Hamara, F. Sundholm, Polymer 38 (1997) 3733.
[12] L.J.A. Siqueira, M.C.C. Ribeiro, J. Chem. Phys. 122 (2005) 194911.
[13] J. Pozuelo, F. Mendicuti, W.L. Mattice, Macromolecules 30 (1997) 3685.
[14] R. Khare, M.E. Paulaitis, Macromolecules 28 (1995) 4495.
[15] M. Mondello, H.-J. Yang, H. Furuya, R.-J. Roe, Macromolecules 27 (1994) 3566.
[16] J.J.L. Cascales, T.F. Otero, J. Chem. Phys. 120 (2004) 1951.
[17] S.J. Weiner, P.A. Kollman, D.T. Nguyen, D.A. Case, J. Comput. Chem. 7 (1986) 230.
[18] T. Shimanouchi, Physical Chemistry VII Molecular Properties, Academic Press, New York, 1970 (Chapter 6).
[19] M. Chhiba, G. Vergoten, J. Mol. Struct. 384 (1996) 55–71.
[20] P. Derreumaux, G. Vergoten, J. Chem. Phys. 102 (21) (1995) 8586–8605.
[21] M. Chhiba, P. Derreumaux, G. Vergoten, J. Mol. Struct. 317 (1994) 171.
[22] P. Derreumaux, M. Dauchez, G. Vergoten, J. Mol. Struct. 295 (1993) 203.
[23] M. Chhiba, G. Vergoten, J. Mol. Struct. 326 (1994) 35.
[24] M. Meziane-Tani, P. Lagant, A. Semmoud, G. Vergoten, J. Phys. Chem. A 110 (2006) 11359–11370.
[25] F. Tristram, V. Durier, G. Vergoten, J. Mol. Struct. 377 (1996) 47–56.
[26] F. Tristram, V. Durier, G. Vergoten, J. Mol. Struct. 378 (1996) 249.
[27] M. Chhiba, F. Tristram, G. Vergoten, J. Mol. Struct. 405 (1997) 113.
[28] Z. Cherrak, P. Lagant, N. Benharrats, A. Semmoud, F. Hamdache, G. Vergoten, Spectrochim. Acta A 61 (2005) 1419–1429.
[29] V. Durier, F. Tristram, G. Vergoten, J. Mol. Struct. (Theochem.) 395–396 (1997) 81–90.
[30] M.J. Frisch, G.W. Trucks, H.B. Schlegel, P.M.W. Gill, B.G. Johnson, M.W. Wong, J.B. Foresman, M.A. Robb, M. Head-Gordon, E.S. Replogle, R. Gomperts, J.L. Andres, K. Raghavachari, J.S. Binkley, C. Gonzalez, R.L. Martin, D.J. Fox, D.J. Defrees, J. Baker, J.J.P. Stewart, J.A. Pople, Gaussian 92, Gaussian, Inc., Pittsburgh, PA, 1993.
[31] H.A. Willis, V.J.I. Zichy, P.J. Hendra, Polymer 10 (1969) 737.
[32] X.S. Xu, Opt. Commun. 199 (2001) 89.
[33] X. Xu, H. Ming, Q. Zhang, Y. Zhang, J. Opt. A: Pure Appl. Opt. 4 (2002) 237–242.
[34] H. Nagai, J. Appl. Polym. Sci. 7 (1963) 1697–1714.
[35] H. Mas Rosemal, S. Mas Haris, S. Kathiresan, Mohan, Pharm. Chem. 2 (2010) 316–323.
[36] A. Neppel, I.S. Butler, J. Raman Spectrosc. 15 (1984) 257–263.
[37] H. Tadokoro, K. Tai, M. Yokoyama, M. Kobayashi, J. Polym. Sci. Polym. Phys. Ed. 11 (1973) 825.
[38] P.R. Sundararajan, P.J. Flory, J. Am. Chem. Soc. 96 (16) (1974) 5025–5031.
[39] D.J. Ward, G.R. Mitchell, Phys. Scr. T57 (1995) 153–160.
[40] M.A. Mora, M.F. Rubio-Arroyo, R. Salcedo, Polymer 35 (5) (1994) 1078–1083.
[41] F. Bosscher, G. ten Brinke, A. Eshuis, G. Challa, Macromolecules 15 (1982) 1364.
[42] E. Schomaker, G. Challa, Macromolecules 22 (8) (1989) 3337–3341.
[43] M. Vacatello, P.J. Flory, Macromolecules 19 (1986) 405.
[44] A. Jain, R.M. Mishra, P. Tandon, V.D. Gupta, J. Macromol. Sci. 45 (2006) 263.
[45] S.K. Dirlikov, J.L. Koenig, Appl. Spectrosc. 33 (1979) 551–555.
[46] S.K. Dirlikov, J.L. Koenig, Appl. Spectrosc. 33 (1979) 555–561.
[47] I. Lipschitz, Polym. Plast. Technol. Eng. 19 (1982) 53.
[48] B. Schneider, J. Stokr, P. Schmidt, M. Mihailov, S. Dirlikov, N. Peeva, Polymer 20 (1979) 705.
[49] M. Mihailov, S.D. Mikov, N. Peeva, Z. Georgieva, Makromol. Chem. 176 (1975) 789.
[50] O.N. Tretinnikov, K. Ohta, Macromolecules 35 (2002) 7343–7353.
[51] O.N. Tretinnikov, Macromolecules 36 (2003) 2179–2182.
[52] S. Havriliak, N. Roman, Polymer 7 (1966) 387.
[53] J. Dybal, S. Krimm, Macromolecules 23 (1990) 1301–1308.
[54] K.J. Thomas, M. Sheeba, V.P.N. Nampoori, C.P.G. Vallabhan, J. Opt. A: Pure Appl. Opt. 10 (2008) 055303.
[55] T.R. Manley, C.G. Martin, Polymer 12 (1971) 524–531.
[56] J.M. O'Reilly, R.A. Mosher, Macromolecules 14 (1981) 602.
[57] H.S. Bu, W. Aycock, B. Wunderlich, Polymer 28 (1987) 1165–1176.
[58] N.O. Tretinnikov, K. Nakao, K. Ohat, R. Iwamoto, Macromol. Chem. Phys. 197 (1996) 753–765.
[59] Y. Grohens, R.E. Prud'homme, J. Schultz, Macromolecules 31 (1998) 2545–2548.
[60] H.S. Shin, Y.M. Jung, T.Y. Oh, T. Chang, S.B. Kim, D.H. Lee, I. Noda, Langmuir 18 (2002) 5953.
[61] D. Emmons, R.G. Kraus, S.S. Duvvuri, J.S. Thompson, A.M. Covington, J. Polym. Sci. B: Polym. Phys. 45 (2007) 358–367.
[62] P.R. Sundararajan, Macromolecules 19 (1986) 415.
[63] R.J. Loncharich, T.R. Schwartz, K.N. Houk, J. Am. Chem. Soc. 109 (1987) 14–23.
[64] P.E. Kireeva, G.A. Shandryuk, J.V. Kostina, G.N. Bondarenko, P. Singh, G.W. Cleary, M.M. Feldstein, J. Appl. Polym. Sci. 105 (2007) 3017–3036.
[65] M.M. Feldstein, T.I. Kiseleva, G.N. Bondarenko, J.V. Kostina, P. Singh, G.W. Cleary, J. Appl. Polym. Sci. 112 (2009) 1142–1165.
[66] J.K. Haken, R.L. Werner, Br. Polym. J. 3 (1971) 263.
[67] J.L. Koenig, A.C. Angood, J. Semen, J.B. Lando, J. Am. Chem. Soc. 91 (1969) 7250.
[68] J.C. Leyte, L.H. Zuiderweg, H.J. Vledder, Spectrochim. Acta 23A (1967) 1397.
[69] A.M. Young, A. Sherpa, G. Pearson, B. Schottlander, D.N. Waters, Biomaterials 21 (2000) 1971–1979.
[70] J. Dong, Y. Ozaki, K. Nakashima, Macromolecules 30 (1997) 1111–1117.
[71] M.-K. Orgill, B.L. Baker, N.L. Owen, Spectrochim. Acta A 55 (1999) 1021–1024.
[72] E.S. Rufino, E.E.C. Monteiro, Polymer 44 (2003) 7189–7198.
[73] J. Ostrowska, A. Narebska, Colloid Polym. Sci. 257 (1979) 128–135.
[74] T. Shimanouchi, I. Nakagawa, Ann. Rev. Phys. Chem. 23 (1972) 217.